Functional Materials Letters
Vol. ~~10~~ 11 No. ~~1~~ 1 (2016) 1650043 (5 pages)

DOI: 10.1142/S1793604716500430

World Scientific
www.worldscientific.com

Revealing the nanodomain structure of silicon oxycarbide via preferential etching and pore analysis

Haolin Wu, Jie Yang, Haibiao Chen*,‡ and Feng Pan†,‡
School of Advanced Materials, Peking University Shenzhen Graduate School
Shenzhen 518055, P. R. China
**chenhb@pkusz.edu.cn*
†panfeng@pkusz.edu.cn

Received 10 March 2016; Accepted 1 April 2016; Published

Preferentially etching either carbon or silica from silicon oxycarbide (SiOC) created a porous network as an inverse image of the removed phase. The porous structure was analyzed by gas adsorption, and the experimental results verified the nanodomain structure of SiOC. This work demonstrated a novel approach for analyzing materials containing nanocomposite structures.

Keywords: Silicon oxicarbide; nanodomain; preferential etching.

Polymer derived ceramics (PDCs) are a special class of ceramic materials which are produced from preceramic polymer precursors.[1] The composition and the microstructure of the PDCs can achieve a high level of homogeneity, in comparison to traditional powder technology. Silicon oxycarbide (SiOC) is one important type of PDCs. SiOC ceramics were found to exhibit excellent thermal stability and creep resistance at high temperatures.[2–4] The homogeneous distribution of carbon in SiOC is believed to enhance the thermal stability and creep resistance. Significant progress has been made in understanding the microstructure of SiOC. It is now widely accepted that the microstructure of SiOC can be described using a nanodomain model formulated by Saha and Raj, in which amorphous silica domains of 1–5 nm are encased in carbon networks.[5] The nanodomain model was based on extensive experimental results from various non-destructive analysis techniques, such as small angle X-ray scattering (SAXS), X-ray diffraction (XRD), Raman spectroscopy, and nuclear magnetic resonance (NMR).[2,5,6] Alternatively, it was previously demonstrated that a porous carbon structure can be prepared from SiOC after removal of silica via chlorination,[7,8] or hydrofluoric acid etching.[6,9] In these studies, the focus was to produce highly porous carbon materials, which exhibited promising performance in gas and energy storage. Gas adsorption technique was employed as a routine technique to analyze the porous carbon structure.

According to the nanodomain model, SiOC can be simplified as a binary nanocomposite composed of silica and carbon. Removing silica will produce a porous carbon, and vice versa. The pores left behind the removed phase present an inverse image of that phase. In this work, carbon and silica were preferentially etched, and the resulted materials were analyzed by gas adsorption separately. The approach introduced in this paper is analogous to the traditional metallography as illustrated in Scheme 1. In traditional metallography, grain boundaries on polished surface are preferentially etched and appeared as dark lines under optical microscope. In our method, one phase is preferentially etched and left pores as "footprints", which was analyzed using gas adsorption to reveal the 3D structure within the original material.

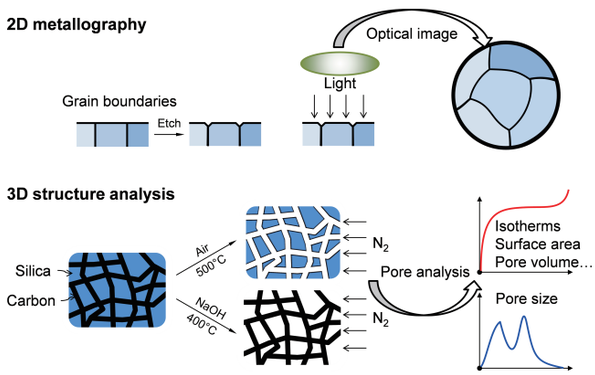

Scheme 1. Analogue of 3D structural analysis via preferential etching and pore analysis to 2D traditional metallography.

‡Corresponding authors.

SiOC ceramic was synthesized from a polysiloxane precursor, which was prepared by cross-linking 20 parts of vinyl-terminated phenyl-methyl polysiloxane (UC-252, Jiaxing United Chemical Co., Ltd.) using 1 part of polymethylhydrosiloxane (Sigma Aldrich) and 0.015 parts of 2 wt% Pt catalyst solution (platinum(0)-1,3-divinyl-1,1,3,3-tetramethyldisiloxane complex solution in xylene, Sigma Aldrich). The cured polysiloxane was pyrolyzed in a tube furnace (MTI Corporation) under nitrogen flow. The furnace was heated from room temperature to 1200°C at 10°C/min and held at 1200°C for 1 h before cooling down. The resulted material was denoted as SiOC1200.

The carbon content of SiOC1200 was measured using a vario EL cube elemental analyzer (Elementar Analysensysteme GmbH), and the oxygen content was measured using a Leco TC-600 oxygen analyzer. The silicon content was calculated by subtracting the carbon content and the oxygen content from 100%. The composition of SiOC1200 was found to be $SiO_{0.9}C_{2.2}$. Since the Si:O ratio is close to one, the SiOC1200 should have a nanodomain structure.[5]

To preferentially etch the carbon phase within SiOC1200, SiOC1200 was heated in a tube furnace with both ends open to air. The thermal etching parameters were first determined from thermogravimetric analysis (TGA) using a Mettler Toledo TGA/DSC 1 unit. In a temperature-ramping experiment, SiOC1200 was heated from 40°C to 900°C at 10°C/min under 50 mL/min of dry air flow. As shown in Fig. 1, sample weight loss starts at around 500°C, and reaches the maximum rate at around 700°C, and stops at around 850°C. It is expected that oxidation of carbon contributed to weight loss, while formation of silica contributed to weight gain. The net weight loss of the sample up to 900°C suggested that carbon oxidation is predominant. Brewer *et al.* studied the oxidation of SiOCs at temperatures ranging from 600°C to 1200°C, and they also observed net weight loss in all samples.[10] Oxidation of SiOC at high temperatures promotes the growth of silica scale.[11] In this study, the thermal etching temperature

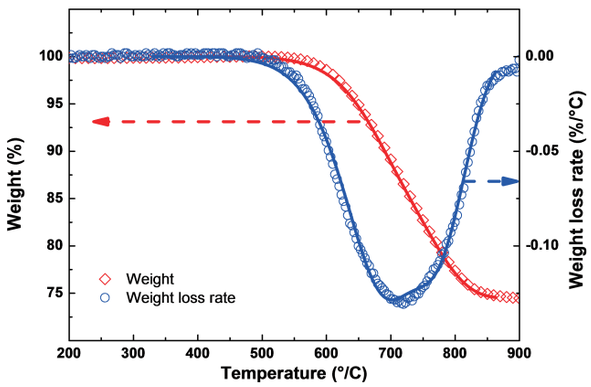

Fig. 1. TGA and DTA data of SiOC1200.

was set to be 500°C, which is sufficient to oxidize carbon easily while limiting silica formation. A series of thermally etched samples were prepared at 500°C and 600°C, after different durations up to 60 h (see supplementary materials). It was found that the thermal etching duration plays a critical role in affecting the specific surface area. When the etching temperature was 500°C, the specific surface area gradually increases as the etching duration increases until reaching a maximum after 40 h. The specific surface area started to decrease if etching continues after 40 h. Similar trend was observed for etching duration at 600°C, with the maximum surface area was reached after only 6 h. We believe that pore elimination due to structure sintering is taking place even at temperature as low as 500°C. Although SiOC ceramics are known for excellent creep resistance, it relies on the presence of the carbon network. During thermal etching, as carbon is gradually removed, silica phase easily flow and sinter. The observed sintering behavior partially supports the nanodomain model. In this study, sample thermally etched at 500°C for 40 h with the highest surface area was selected for further analysis, and it was denoted as SiO500.

To preferentially etch the silica phase within SiOC1200, SiOC1200 was thoroughly mixed with sodium hydroxide (NaOH) in a ratio of 1:4. The mixture was placed in a nickel boat and heated in a tube furnace under nitrogen flow. The furnace was heated from room temperature to 400°C at 10°C/min and held at 400°C for 1 h before cooling down. At this temperature, NaOH is molten and reacts with silica while it should not attack carbon.[12] The product was washed with diluted hydrofluoric acid and copious deionized water, and then dried in a vacuum oven. The resulted material was denoted as C400.

XRD was carried out on a Bruker D8 Advance with Cu-Kα radiation and the results for all three samples are shown in Fig. 2(a). The SiOC1200 showed a weak peak at 26.6°, which is from the reflection of the (002) planes of graphite. There is another weak and very broad peak at around 43° corresponding to the diffraction from graphene sheets, characteristic for amorphous and disordered carbons.[13] After thermal etching, a broad peak appeared at around 22° for SiO500 and it can be assigned to α-cristobalite.[7] As the carbon barrier was removed, silica can start to sinter and crystalize under the thermal etching condition. After removal of silica phase, the XRD pattern of C400 showed broad peaks at around 23° and 43°, which should be assigned to the (002) and (101) planes of graphite. The shifting of (002) peak to lower 2θ suggests the graphene layer spacing increased from 0.335 nm to 0.384 nm after the NaOH etching process. The stacking thickness along the (002) direction was calculated to be 0.89 nm using Scherrer equation, corresponding to 3–4 stacked layers. The result agrees well with the nanodomain model.

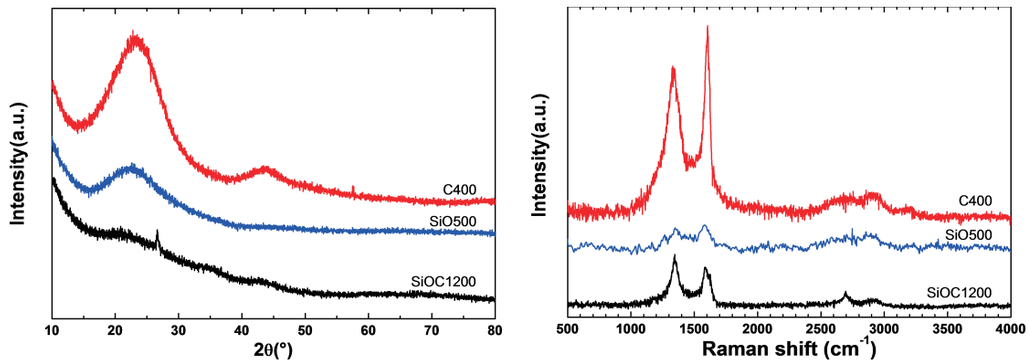

(a) (b)

Fig. 2. (a) XRD and (b) Raman analysis.

Raman spectra were collected using a Horiba modular Raman system consisting of an optical microscope (Olympus BX41), a diode laser source ($\lambda_0 = 532$ nm, LEO Photoelectric Co., Ltd), an iHR320 spectrometer with a Synapse CCD detector (Horiba Instruments Inc). The Raman spectra of three materials are shown in Fig. 2(b). Note that the intensity of the spectra was not normalized for a purpose. The intensity of the spectrum of C400 is the strongest, followed by that of SiOC1200. The intensity of the spectrum of SiO500 is the weakest. The Raman spectra verify the presence of graphitic carbon within the structure of SiOC1200. When carbon is removed as in sample SiO500, the Raman response almost disappeared. When silica is removed, carbon layers had a chance to reorient to a more organized arrangement, resulting in stronger response in C400. The D band at around 1340 cm^{-1} originates from the 6-fold ring breathing mode vibration and the G band at around 1580 cm^{-1} originates from the in-plane stretching mode vibration of sp2 bonds along the chain direction. The ratio of the intensity of D band to that of G band can be used to estimate the size of the graphite crystallite size. Using the model developed by Tuinstra and Koenig,[14,15] the sizes of graphite crystallites in SiOC1200 and C400 were estimated to be 1.20 nm and 1.98 nm, respectively. These values were consistent with the nanodomain model of the SiOC materials, and they also confirm that graphite crystallites grew larger after the silica phase is removed.

The nitrogen physisorption isotherms of the samples were measured using a Micromeritics ASAP 2020 unit. The specimen was manually degassed on the analysis port to minimize possible contaminations. The specific surface area (S_{BET}) was calculated using the BET (Brunauer–Emmett–Teller) method. The total pore volume (V_P) was taken from the adsorbed volume at the highest measured relative pressure which was close to unity. The pore size distribution was derived using the density function theory (DFT) method with a nitrogen-on-carbon model. The nitrogen physisorption isotherms of all samples are shown in Fig. 3(a). SiOC1200 is close to non-porous and exhibit very low nitrogen adsorption volume. The specific surface area of SiOC1200 was only 10 m^2/g as calculated using the BET model, and the pore volume was only 0.02 cm^3/g. After either thermal etching or NaOH etching, the specific surface area and the pore volume

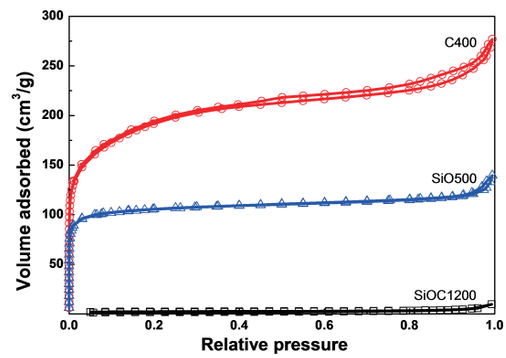

(a)

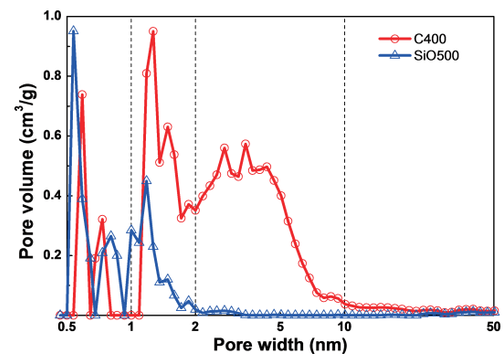

(b)

Fig. 3. (a) Nitrogen adsorption isotherms and (b) DFT pore size distribution.

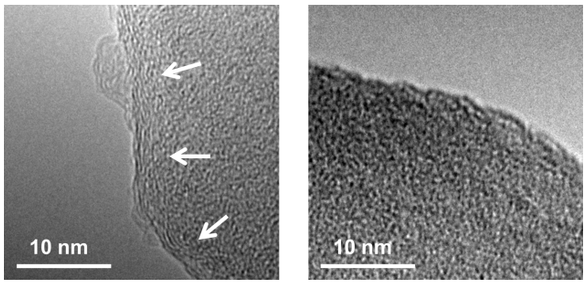

(a) (b)

Fig. 4. TEM of (a) SiO1200 and (b) SiO500.

increased significantly. The isotherm of the thermally etched sample, SiO500, resemble type I isotherm as classified by IUPAC. The adsorption at very low pressure was contributed by micropore filling. The adsorption volume in medium to high pressure range is negligible. The BET specific surface area, total pore volume, and average pore width of SiO500 were calculated to be 410 m^2/g, 0.22 cm^3/g, and 2.1 nm, respectively. Apparently, removing carbon phase from SiOC creates mostly micropores within the material. The size of the pores reflects the original dimension of the carbon clusters within the structure. Note that the pore width of 2.1 nm was calculated by the cylindrical model by convention ($4V_P/S_{BET}$). If calculated using the slit model ($2V_P/S_{BET}$), the pore width will be 1.1 nm, which is quite consistent with the carbon crystallite size calculated from the Raman data. The isotherm of the sample etched in NaOH, namely C400, resembles a type IV isotherm as classified by IUPAC. The C400 material contains a large content of micropores, and some mesopores as indicated by the adsorption at medium pressure range and hysteresis. The BET surface area, total pore volume, and average pore width of C400 were calculated to be 697 m^2/g, 0.43 cm^3/g, and 2.5 nm, respectively. Ideally the surface areas of SiO500 and C400 should be identical since they should be equal to the interface area between the silica and carbon phase in the original SiOC1200. However, the specific surface area of C400 is higher, probably because the silica phase in SiO500 experienced an ongoing sintering process as mentioned earlier, and NaOH also created additional pores within the carbon phase of C400. Considering the densities of the carbon phase and the silica phase are similar, the large pore volume of C400 suggests that silica phase in SiOC occupied larger volume than carbon. The average domain size of the silica phase is also likely larger than that of the carbon phase.

The DFT pore size distribution in Fig. 3(b) provides more detailed information on the nanostructure of the materials. For sample SiO500, all pores are smaller than 2 nm, indicating that this material is almost exclusively microporous. The pore width in SiO500 corresponds to the wall thickness of the carbon network SiOC1200. If assuming the carbon layer spacing is around 0.384 nm, the carbon wall consists of no more than six layers of graphene. This result is consistent with the XRD analysis and supports the nanodomain model. For sample C400, most pores are in the range of 1–2 nm and 2–10 nm. The pores present a reverse image of the removed silica nanodomains. The results suggest that most silica nanodomains are in the range of 1–2 nm and 2–10 nm. This is consistent with the nanodomain model of SiOC. However, it is noteworthy that if NaOH also etched carbon, pores from neighboring nanodomains can connect and form larger pores. Nevertheless, it is most likely that the dimension of the silica nanodomains tend to be larger than the wall thickness of carbon. Both results are consistent with the assumption in the nanodomain model of SiOC.

High resolution transmission microscopy (HRTEM) analysis of the material was performed on an FEI Tecnai G2 F30. The TEM images of SiOC1200 and SiO500 are shown in Fig. 4. The SiOC1200 material show very homogenous morphology even under high resolution TEM, suggesting that the material is both chemically and structurally homogenous. Layered carbon structure can be seen on the surface of the particles in SiOC1200, while similar structure cannot be found in the thermally etched SiO500 since carbon is removed. Layered carbon structure can also be seen in sample C400 (see supplementary materials).

In summary, we report a new technique to directly verify the nanodomain structure of SiOC via preferential etching of a selected phase and performing pore analysis on the resulted porous structures. By thermal etching at 500°C, carbon was preferentially removed, leaving micropores within the material. By NaOH etching at 400°C, silica was preferentially removed, leaving both micropores and mesopores within the material. Pore analysis by nitrogen adsorption revealed that the width of the created pores is consistent with the nanodomain model. The pore analysis results also self-agree well with the XRD and Raman characterization results. This work initiates a new perspective in analyzing the bulk structure of very homogenous nanocomposite structure which is common in many PDCs.

Acknowledgment

The research was financially supported by Guangdong Innovation Team Project (No. 202013N080), and Shenzhen Science and Technology Research Grant (Nos. JCYJ20150518092933435 and JCYJ20150626110958181).

References

1. P. Colombo, G. Mera, R. Riedel and G. D. Sorarù, *J. Am. Ceram. Soc.* **93**, 1805 (2010).

2. C. G. Pantano, A. K. Singh and H. Zhang, *J. Sol–Gel Sci. Technol.* **14**, 7 (1999).
3. S. Walter, G. D. Soraru, H. Bréquel and S. Enzo, *J. Eur. Ceram. Soc.* **22**, 2389 (2002).
4. T. Rouxel, G.-D. Soraru and J. Vicens, *J. Am. Ceram. Soc.* **84**, 1052 (2001).
5. A. Saha, R. Raj and D. L. Williamson, *J. Am. Ceram. Soc.* **89**, 2188 (2006).
6. R. Peña-Alonso, G. Mariotto, C. Gervais, F. Babonneau and G. D. Soraru, *Chem. Mater.* **19**, 5694 (2007).
7. C. Vakifahmetoglu, V. Presser, S.-H. Yeon, P. Colombo and Y. Gogotsi, *Microporous Mesoporous Mater.* **144**, 105 (2011).
8. A. Meier *et al.*, *Microporous Mesoporous Mater.* **188**, 140 (2014).
9. R. Pena-Alonso, G. D. Soraru and R. Raj, *J. Am. Ceram. Soc.* **89**, 2473 (2006).
10. C. M. Brewer, D. R. Bujalski, V. E. Parent, K. Su and G. A. Zank, *J. Sol–Gel Sci. Technol.* **14**, 49 (1999).
11. S. Modena, G. D. Soraru, Y. Blum and R. Raj, *J. Am. Ceram. Soc.* **88**, 339 (2005).
12. M. Lillo-Ródenas, D. Cazorla-Amorós and A. Linares-Solano, *Carbon N. Y.* **41**, 267 (2003).
13. H. Fukui, H. Ohsuka, T. Hino and K. Kanamura, *J. Electrochem. Soc.* **158**, A550 (2011).
14. F. Tuinstra, *J. Chem. Phys.* **53**, 1126 (1970).
15. A. Ferrari and J. Robertson, *Phys. Rev. B* **61**, 14095 (2000).